Effect of Unstable Density Gradients on Back-Mixing in a Reciprocating Plate Column

Kannan Aravamudan and Malcolm H. I. Baird
Dept. of Chemical Engineering, McMaster University, Hamilton, Ontario L8S 4L7, Canada

Axial dispersion coefficients were measured in the continuous phase in a 5-cm-dia. Karr column, operated cocurrently with the system kerosene(d)-water(c). The effect of unstable density gradient in the continuous phase was studied by injecting a steady stream of sodium chloride solution as a tracer near the top of the column. The effects of energy dissipation due to unstable density gradient, mechanical agitation, and the flow of the dispersed phase were investigated as the three principal variables, and two plate spacings (2.55 and 5.10 cm) were also employed. The axial dispersion results were correlated in terms of a weighted power-law model based on Kolmogoroff's mixing length concept and incorporating contributions due to each of the three modes of energy dissipation. Axial mixing was significantly increased in the presence of unstable density gradients even though these contributed very little (typically less than 1 mW/kg) to the total specific energy dissipation rate.

Introduction

Until about 35 years ago, extraction columns were designed on the assumption that the two liquid phases moved in plug flow. Since then it has been realized that in most practical columns, axial mixing tends to reduce the concentration driving forces below the values predicted from the classically constructed plug-flow operating lines (Treybal, 1963). Therefore, it is necessary to include axial mixing effects in column design, and the various approaches have been reviewed by Pratt and Baird (1983). These predictive models require a parameter for the magnitude of axial mixing. In columns containing discrete compartments, the stagewise approach employs the backflow ratio as a mixing parameter. Columns in which discrete stages are not readily identifiable, such as packed columns, are termed "differential contactors," and the rate of axial mixing is described by the axial flux as follows:

$$N = -E\frac{dc}{dz}. \tag{1}$$

The axial dispersion coefficient E is several orders of magnitude greater than the molecular diffusion coefficient of the solute. In the continuous liquid phase it is determined by levels of turbulence and circulation, and by wakes of liquid entrained behind droplets. In the dispersed (droplet) phase it is strongly affected by drop nonuniformity, which gives rise to forward mixing (Rod, 1966).

This article is concerned with continuous phase axial mixing in a Karr reciprocating plate column. It includes for the first time an examination of the role of unstable density gradients as well as two-phase flow and mechanical agitation.

Literature Review

The Karr column was developed about 40 years ago (Karr, 1959) and has since been applied mainly in the pharmaceutical industry, in diameters up to 1.7 m (Lo and Prochazka, 1983; Baird et al., 1994). Since the perforated plates have an open area fraction (S) of about 0.6, Karr columns behave as differential contactors and axial mixing has been described in terms of the axial dispersion model (Eq. 1). Quite extensive data are available on the values of E in Karr reciprocating plate columns of diameter up to 15 cm. Sources have been reviewed by Aravamudan (1995), and they include the work of Kim and Baird (1976) on a 5-cm-diameter column, Hafez et al. (1979) on a 15-cm-diameter column, and Karr et al. (1987), who reported some data from a 50.8-cm-diameter column. Most of the previous research on axial mixing has been under nonmass-transfer conditions, but Bensalem (1985) car-

Correspondence concerning this article should be addressed to M. H. I. Baird.
K. Aravamudan is currently with the Chemical Engineering Dept., I. I. T., Kanpur, India 20816.

carried out extensive work on a 7.62-cm-diameter Karr column with mass transfer using the system water(c)-acetone-toluene(d). He found that different correlation equations for axial dispersion were necessary for the cases of (1) no mass transfer, (2) mass transfer ($c \rightarrow d$), and (3) mass transfer ($d \rightarrow c$).

An early modeling approach to axial dispersion was that of Novotny et al. (1970), who assumed that the liquid in a pulsed or reciprocating plate column consisted of a well-mixed region near the plates and a more poorly mixed region between the plates. Nemecek and Prochazka (1974) applied the model to two-phase systems. The two-zone concept was refined by Stevens and Baird (1990), who successfully compared it with results from several different literature sources, but only for single-phase conditions. When two liquid phases are passed through an open structure type of column (of which the Karr column is an example), large-scale circulation currents are induced by the dispersed phase. Rosen and Krylov (1967, 1974) introduced the concept of "transverse nonuniformity" in their studies of these effects. They proposed a simple additive equation for axial dispersion coefficients:

$$E = E_a + E_{tn}. \tag{2}$$

The term E_a is proportional to the level of agitation and represents the effect of mechanically produced turbulence. The second term E_{tn} was strongly dependent on dispersed phase flow but *inversely* affected by agitation. Therefore Eq. 2 could reproduce the observed trends that E is large at zero agitation, then passes through a minimum as agitation is increased. At high agitation levels, E approaches E_a.

Attractively simple models for mixing and other hydrodynamic effects are obtainable from Kolmogoroff's (1941) approach to turbulence. It is postulated that at high Reynolds numbers there exists a range of high wave-numbers corresponding to eddies that are in dynamic equilibrium and unaffected by viscosity.

$$E = l^{4/3}\epsilon_t^{1/3}. \tag{3}$$

Dimensional analysis leads to the simple relationship above, where ϵ_t refers to the total energy dissipation per unit mass of fluid, expressed either as W/kg in S.I. units or cm^2/s^3 in c.g.s. units. The term l is a mixing length, characteristic of the effective eddy size. Kostanyan et al. (1979) used a form of Eq. 3 to correlate E values in reciprocating plate columns having rectangular perforations in the plates, with ϵ_t being calculated from the mechanical energy input. Baird and Rice (1975) adapted Eq. 3 to mixing in open and unagitated spray columns and bubble columns, where energy dissipation (ϵ_d) is due to the flow of the dispersed phase. They showed that data from several different sources were consistent with Eq. 3 using the following substitutions:

$$\epsilon_t = \epsilon_d = \frac{u_d g |\rho_c - \rho_d|}{\rho} \tag{4}$$

$$l = 0.455D. \tag{5}$$

More refined models based on the detailed structure of the two-phase flow in open columns have since been proposed, but Kawase and Moo Young (1991) point out in their review that the simple equation of Baird and Rice (1975) gives almost the same predictions as the later models.

Unstable Density Gradients

An unstable density gradient is said to exist in the continuous phase when its density increases with height in the column. The continuous phase then tends to mix vertically, and this effect will augment the mixing due to mechanical agitation and/or flow of the dispersed phase. Although the unstable density effect in extraction columns was only explicitly recognized a few years ago (Cusack and Karr, 1991), there is some evidence of its existence from earlier literature. Rosen and Krylov (1967) discuss the possibility of axial circulation in the heavy liquid phase created by sharp decreases in density due to extraction. They cite the study of Sege and Woodfield (1954) who investigated the extraction of uranyl nitrate. Bensalem (1985) reported higher axial mixing under mass-transfer conditions ($d \rightarrow c$) than under ($c \rightarrow d$) and attributed this to circulation effects with large drops, but the same trend could also be expected from unstable density gradients. Dongaonkar et al. (1991) reported that mixing was greater under mass-transfer conditions than in the absence of mass transfer in a Kühni column; they attributed the enhancement to entrained wakes behind droplets, but in this case the results also could be due, at least in part, to unstable density gradients.

The direct measurement of axial mixing in the presence of controlled unstable density gradients was first carried out by Holmes et al. (1991) in a 7.62-cm-diameter Karr column, operated with an upward flow of water and continuous injection of brine near the top of the column. It was found that in the absence of mechanical agitation the flux was proportional to the 3/2 power of the brine concentration gradient. Under these conditions the effective axial dispersion coefficient could be defined in terms of Eq. 3 with the specific buoyant energy dissipation rate given by

$$\epsilon_b = \frac{u_c g(\rho_c - \rho_{co})}{\rho_c}, \tag{6}$$

where ρ_c refers to the local density of the continuous phase and ρ_{co} is the density in the absence of solute.

Baird and Rama Rao (1991) studied a 5.08-cm-diameter Karr column with the brine–water system and also a cold–hot water system to examine the effects of very small density gradients. The axial dispersion data for these single-phase systems were fitted to an expanded form of Eq. 3 in which E was expressed as follows:

$$E = \left[l_m + (l_b - l_m)\left(\frac{\epsilon_b}{\epsilon_t}\right)^{n_b} \right]^{4/3} (\rho_m + \rho_b)^{1/3}. \tag{7}$$

The energy dissipation rates ϵ_b and ϵ_m are given, respectively, by Eq. 6 and the following expression for reciprocating plate columns (Hafez and Baird, 1978):

$$\epsilon_m = \frac{2\pi^2}{3} \frac{(1-S^2)}{C_o^2 S^2} \frac{(Af)^3}{H} \tag{8}$$

Equation 7 contains three fitted parameters that were evaluated by Baird and Rama Rao (1991) by a statistical fit with their data. The mixing lengths, l_m for mechanical energy and l_b for buoyant energy, were, respectively, 0.301 cm and 4.02 cm, and the weighting exponent n_b was 0.34. The buoyant mixing length is $0.8D$ as compared to the earlier work of Holmes et al. (1991) in which the fitted value of l_b was 5.3 cm or 0.7 D. Other results of Baird et al. (1992) and Baird and Legree (1994) confirm that l_b is of the same order as column diameter. The much smaller value of l_m denotes that the mechanically produced eddies have dimensions similar to those of the webs of metal between the perforations in the plates.

The preceding observations show that unstable density gradients can have a significant effect on axial dispersion. The energy dissipation rates calculated from Eq. 6 are very low, typically in the order of 0.5 mW/kg compared with mechanical agitation rates typically in the order of 1,000 mW/kg. However, the higher values of the mixing length l_b as compared with l_m allow unstable density gradients to increase dispersion significantly, even under well agitated conditions. In the present work, the additional effects of two-phase (liquid–liquid) flow as well as mechanical agitation and unstable density gradient are studied. The energy dissipation rate due to the dispersed-phase flow is given by Eq. 4.

Experimental

The column and ancillaries are shown in Figure 1. The column itself was 5.08-cm (2-in.) nominal internal diameter and 1.8-m total height, constructed of flanged glass sections. Essential dimensions of the column and the plates are given in Table 1. The plate stack could be reciprocated sinusoidally at frequencies up to 5 Hz by means of a variable-speed motor (VSM in Figure 1) and yoke drive (Y) located above the column. The operating stroke was set at 3.10 cm and not varied during the experiments. It has been generally found (Baird et al., 1994) that agitation effects can be expressed as the frequency-stroke product, Af. For example Eq. 8 shows that mechanical energy dissipation varies as $(Af)^3$. This equation is valid at operating strokes in excess of about 2 cm, which are normally used in Karr columns. Therefore the variations of f were used to vary ϵ_m.

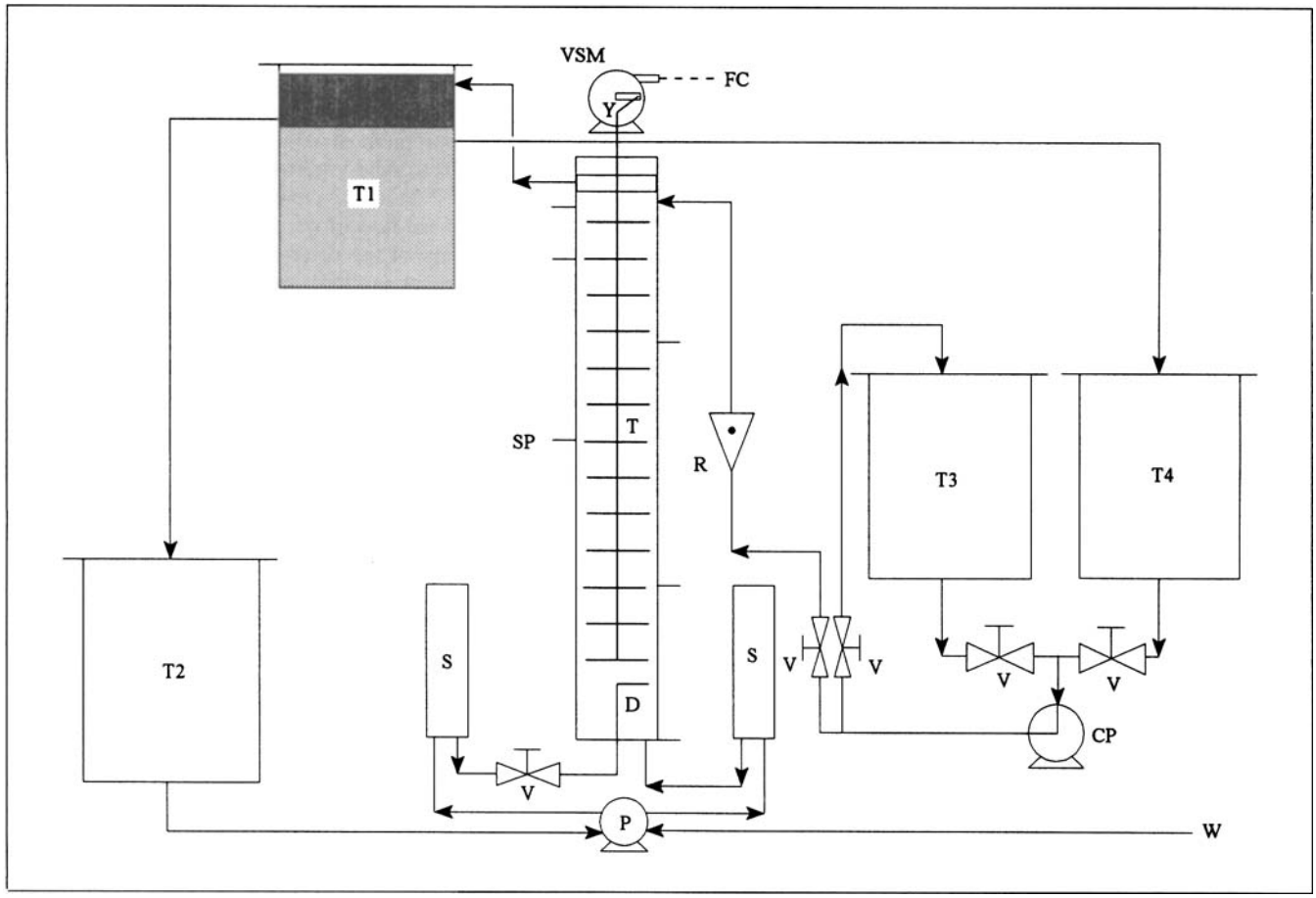

Figure 1. Experimental setup for back-mixing experiments.

CP—centrifugal pump; D—distributor; FC—frequency controller; P—pump; S—surge cylinder; SP—sample port; T—plate-stack; T1—two phase tank; T2—isopar storage tank; T3, T4—NaCl tanks; V—flow control valve; VSM—variable speed motor; W—tap water storage; Y—yoke.

Table 1. Important Dimensions of the RPC Used in this Study

No.	Column Variable	Characteristic	Dimension
1	Plate	Outer diameter	4.83 cm
2		Hole diameter (d_h)	13.56±0.01 mm
3		Thickness (d_t)	1.54±0.02 mm
4		Fractional free area (S)	0.56
5	Spacer	Outer diameter	9.52±0.02 mm
6		Length	2.55 cm
7	Glass Section	Length	15/30 cm
8		Inner diameter (D)	5.08 cm
9		Thickness	7.8±0.1 mm

The light (dispersed) liquid phase was Isopar M (Imperial Oil of Canada), a purified form of kerosene with density 985.3 kg/m^3, viscosity 2.4 mPa·s and mean molecular weight 191. This was fed through a duplex metering pump (P on Figure 1) through a pulsation dampener (S) to a perforated ring distributor (D) at the base of the column. The aqueous (continuous) feed, tap water with a density of 997.2 kg/m^3 at ambient conditions, was fed through the second channel of the metering pump (P) and also entered at the base of the column. The interfacial tension of the liquid–liquid system was determined to be 50 mN/m.

In order to study the effects of unstable density gradient, a metered flow of sodium chloride tracer solution was fed by a centrifugal pump (CP) to a point near the top of the column. The tracer system comprised of feed tank (T3) and receiving tank (T4). The diluted tracer from the two-phase receiving tank (T1) was recycled to tank (T3) through tank (T4) and made up to the feed concentration. Typically, the concentration of the feed brine was 7% by mass with a density 1,040 kg/m^3. For the sodium chloride/water system, the solution density is a linear function of sodium chloride concentration.

$$\rho_c = \rho_{co} + 0.70c. \tag{9}$$

Some tests were also carried out under "neutrally buoyant" conditions in which the density of the feed brine was adjusted to the same value as water by adding sufficient methanol to a 3% solution of sodium chloride.

Back-mixing of the sodium chloride under steady-state conditions was measured by taking samples from several points beneath the tracer entry, as shown in Figure 2. Steady-state conditions were initially established by operating the column for about three residence times of the continuous phase. Samples of approximately 15 mL were then taken at 3-min intervals from different points using a staggered arrangement and it was established that the steady flow profiles were not disrupted by this operation. The sodium chloride samples were analyzed by a precalibrated electrical conductivity meter (CDM3 Radiometer, Copenhagen). A separate calibration chart was used for the neutrally buoyant studies in which methanol was added to the tracer feed.

The principal operating variables in the experimental scheme were dispersed phase flow ($0 < u_d < 0.38$ cm/s), agitation frequency ($0 \le f < 3.5$ Hz), and the plate spacing H (2.55 and 5.10 cm). In addition, each concentration profile measurement provided two to three values of the density gradient and two to three different values of ϵ_b.

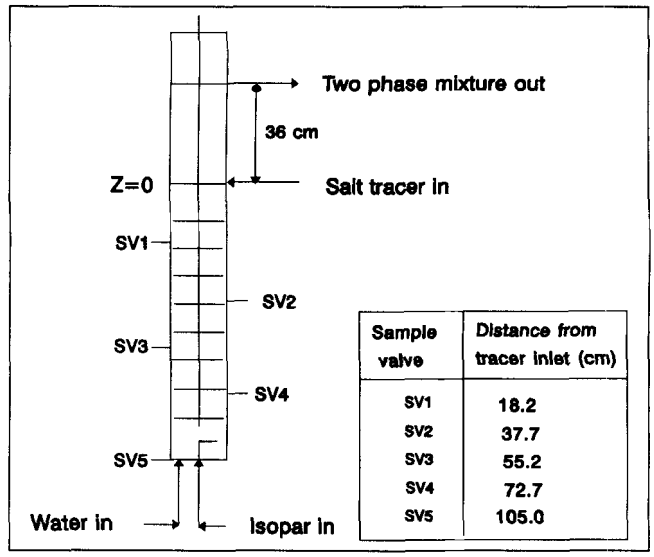

Figure 2. Sampling arrangement and back-mixing scheme.

Data Processing and Model Development

The governing equation for steady one-dimensional back-mixing of tracer in the continuous phase, in the absence of mass transfer, is

$$u_c c - E\frac{dc}{dz} = 0. \tag{10}$$

For the case where E is a constant, this equation can easily be integrated, providing the well-known concentration profile that decays exponentially with distance measured back from the tracer injection point. However, in the presence of unstable density gradient, E cannot be assumed constant, and instead it must be measured from the slopes of the concentration profiles:

$$E = u_c c \Big/ \frac{dc}{dz}. \tag{11}$$

Manual slope measurements are prone to inaccuracy, and after various trials including the use of spline methods, it was decided (Aravamudan, 1995) to fit each measured concentration profile with a polynomial function, and then calculate the local slopes by differentiating the polynomial. Figure 3 shows typical data points and fitted curves. Slopes and concentrations were evaluated at each sample point and used in Eq. 11 to calculate the local values of E.

The first modeling approach to be tried was based on an extension of Eq. 7, introducing the three types of energy dissipation into the weighted expression for the mixing length. The following equation is obtained:

$$l = l_m + (l_b - l_m)\left(\frac{\epsilon_b}{\epsilon_t}\right)^{n_b} + (l_d - l_m)\left(\frac{\epsilon_d}{\epsilon_t}\right)^{n_d}. \tag{12}$$

The three energy dissipation rates can be calculated, and there are five adjustable parameters, namely the three mixing

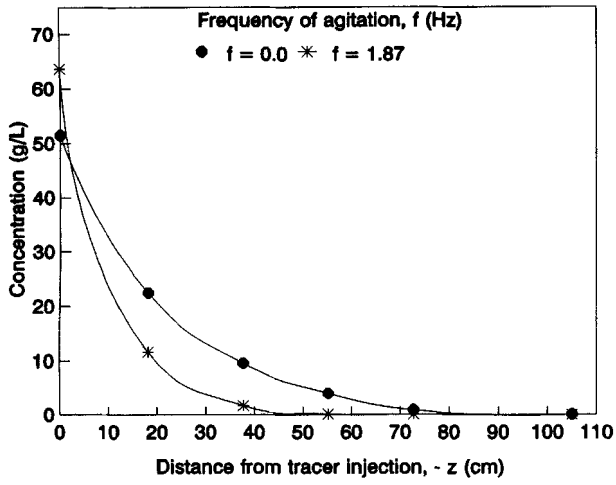

Figure 3. Typical tracer concentration profiles.

lengths and the two weighting exponents n_b and n_d. This equation retains the important property that when one form of energy becomes zero, its contribution to the overall mixing length also disappears. However, on the basis of tests against experimental data (Aravamudan, 1995) it was concluded that Eq. 12 did not allow for strong effects of circulation induced by the two-phase flow at low agitation levels. Accordingly the dispersed-phase flow contribution in Eq. 12 had to be modified. The reasoning on which the modification was based is discussed below.

Liquid circulation effects

The introduction of the dispersed phase, especially under nonagitated conditions, produces a significant change in the hydrodynamics and consequently back-mixing in the continuous phase. The rising drops agitate the liquid by the creation of turbulent eddies combined with a steady circulating flow (Walter and Blanch, 1983). The dispersed phase tends to rise along the core of the column and the continuous phase is also translated in the core, returning along the annulus and setting up a recirculating flow. The recirculation currents are especially severe in the absence of plate oscillation and depend strongly on the plate spacing and the dispersed phase flow rate. Hence, it was decided to modify the mixing length term in order to incorporate the synergistic effect of these two variables. To facilitate the modeling process especially under zero and low agitation, each stage of the Karr column was visualized to be a bubble (or spray) column.

It is proposed that the dimensionless length of the circulation cell (β^*) is a measure of circulation inside each compartment. This also represents the extent of back-mixing in the continuous phase. The longer the circulation cell, the more severe is the back-mixing. With increasing plate spacing, the length of the circulation cell will increase. This approach, visualizes only one circulation cell between each pair of plates. This is in contrast to earlier works in unbaffled bubble columns where the column was postulated to comprise of multiple circulation cells of height equal to column diameter (Joshi and Sharma, 1979). Devanathan et al. (1990), in a detailed flow-mapping study in bubble columns using a radioactive particle-tracking technique observed that there was a single toroidal circulation cell with liquid ascending along the column center and descending along the wall. At low gas velocities they observed two such cells. However, the second cell was confined to the entry region of the dispersed phase. It is assumed in this work that β^* is proportional to $1+H/D$. Incorporating β^* into the overall mixing length leads to

$$l_d = l_{do}\beta^* = l_{do}\left(1+\frac{H}{D}\right). \tag{13}$$

With increasing dispersed phase flow rate, radial distribution of the drops improves and the circulation currents are weakened. Since the drops occupy the entire cross-sectional area of the column the return flow of the continuous phase along the column walls is inhibited. Therefore, there is a sharp drop in the back-mixing in the continuous phase. It is assumed that this decrease is exponential with respect to ϵ_d.

Introducing plate oscillation drastically alters the mechanism of back-mixing in the continuous phase. Eddy (turbulent) diffusion effects become more important. Back-mixing is now caused mainly by the presence of turbulent eddies generated by the agitation due to the oscillating plates and by the dispersed phase drops. By the same token, circulation effects are suppressed by increased radial transport of momentum. The intense mechanical agitation results in a denser dispersion of drops within each stage, thereby further dampening the circulation effects and greatly improving the radial uniformity. Hence, an expression is needed that takes into account the influence of dispersed phase flow rate (or equivalently ϵ_d) at zero agitation and also the effect of agitation (or equivalently ϵ_m) when applied. Hence the mixing length coefficient l_{do} given in Eq. 13 may be further resolved to incorporate the effects of plate oscillation and dispersed phase flow rate as follows:

$$l_{do} = l^*_{d0}\exp\left(-\frac{\epsilon_d}{\epsilon_{mo}+\epsilon_m}\right), \tag{14}$$

where ϵ_{mo} is a constant parameter. This additional fitting parameter is the energy term that controls the threshold effect of mechanical agitation in reducing transverse circulation effects. The dispersed phase contribution to mixing length can therefore be interpreted as qualitatively equivalent to the "transverse nonuniformity" term proposed by Rosen and Krylov (1967, 1974). The important difference is that in this work the energy-dissipation rates, which are readily obtainable, are allowed to play a major role in the model. So the final expression for the dispersed-phase mixing length l_d becomes

$$l_d = l^*_{do}\left(1+\frac{H}{D}\right)\exp\left(-\frac{\epsilon_d}{\epsilon_{mo}+\epsilon_m}\right). \tag{15}$$

The final expression for the mixing length can therefore be represented as

$$l = l_m + (l_b - l_m)\left(\frac{\epsilon_b}{\epsilon_d}\right)^{n_b} + \left[l^*_{do}\left(1+\frac{H}{D}\right)\exp\left(-\frac{\epsilon_d}{\epsilon_{mo}+\epsilon_m}\right) - l_m\right]\left(\frac{\epsilon_d}{\epsilon_t}\right)^{n_d}. \tag{16}$$

Comparison Between Data and Model

Experimental values of l are calculated from measured values of E and the total energy-dissipation rate, on the basis of Eq. 3. Measurements have been carried out with all possible combinations of the three forms of energy, as follows:

(a) Three sets of data for which only one of the three forms of energy dissipation present.

(b) Three sets of data with two of the three forms of energy dissipation present.

(c) A large set of data with all three forms of energy dissipation present.

The number of data points in each set and the ranges of variation of the energy-dissipation rates are summarized in Table 2. The first and fifth lines of Table 2 are comparable to the experiments of Holmes et al. (1991) and Baird and Rama Rao (1991).

Estimation of parameters

The parameters of the model were evaluated by using General Algebraic Modeling System (GAMS) software. Since the model is highly nonlinear and multiple solutions corresponding to local minima are possible, it was decided to check the predictions from GAMS by using another software that uses the standard Levenberg–Marquardt technique. The predictions from POLYMATH were almost identical to that from GAMS. (POLYMATH's capacity was limited to only five variables.) Hence, by fixing one of the variables, the remaining ones were verified. The parameter predictions were independent of the variable whose value was fixed from the GAMS estimate. Further the check on 95% confidence intervals (CI) from POLYMATH indicated that all the parameters in the model were significant. None of the parameters had CIs that overlapped zero.

The fitted values of the six parameters in Eq. 16 have been obtained by regression of all the 55 data points, and are given in Table 3 along with confidence intervals. Where applicable, parameters from the single-phase analysis of Baird and Rama Rao (1991) are shown for comparison. Analysis of the present data with only one form of energy dissipation (see (a)) showed that the measured mixing lengths were in reasonable agreement with the regression values.

Statistical analysis of results

The residuals (e_i) were defined as the difference between the ith data point and the model prediction. The sum of the square of the residuals defined as

$$\sum_{i=0}^{N_d} (l_{\text{model}} - l_{\text{expt}})_i^2 \tag{17}$$

was minimized in the optimization program to estimate the model parameters. The number of data points N_d as mentioned earlier is 55. The sum of the square of residuals improved from 2.39 to 1.32 when Eq. 12 was modified to Eq. 16 at the cost of an additional adjustable parameter, viz., ϵ_{mo}.

The root-mean-square deviation (s) defined as

$$s = \sqrt{\frac{\sum_{i=0}^{N_p} (E_{c,\text{model}} - E_{c,\text{expt}})_i^2}{N_d - N_p}} \tag{18}$$

was used in the analysis of residuals as described below. The value of s improved from 0.22 (Eq. 12) to 0.16 (Eq. 13).

In fitting this model it was assumed that the residuals are random, independent, have zero mean, same variance, and follow a normal distribution. The following methods were adopted to test the sufficiency of the model as recommended by Draper and Smith (1981):

1. The residuals were represented in a normal plot (Figure 4) using MINITAB. A linear relationship with a high correlation (0.992) was obtained, thereby confirming that the residuals are random and normally distributed.

2. Ninety-five percent of the unit normal deviates expressed as e_i/s (where s is defined from Eq. 18) should fall within approximately ± 2.01, corresponding to the 95% limits of a t distribution with 49 degrees of freedom. In this work, 52 out of the 55 data points corresponding to 94.5% of the unit normal deviates fell in this category. Using a normal distribution, since there are a large number of data points, leads to the criterion that 95% of the unit normal deviates should be within ± 1.96. This criterion, being more stringent than the t test, led to the identification of five outliers which are tagged as O_1 to O_5 in the normal plot (Figure 4).

From the preceding results it can be concluded that the errors are random with a normal distribution. The residuals corresponding to the outlier were examined with the following results:

1. Outliers 1 and 2 came from the same experiment. These points correspond to high values of ϵ_b (3.568 and 7.902

Table 2. Summary of Energy Ranges Studied

No. of Data Points	Form and Ranges of Energy Dissipation Rates, mW/kg		
	Buoyant (Eq. 6)	Dispersed Phase (Eq. 4)	Mechanical (Eq. 8)
3	0.24–0.65	0	0
2	0*	3.5–6.8	0
1	0*	0	26
12	0.009–0.96	3.5–6.8	0
13	0.015–0.73	0	27–1,700
4	0*	3.5–6.8	24.5–148
20	0.017–1.0	3.5–6.9	24.5–1,730

Note: *refers to data with neutrally buoyant solutions.

Table 3. Model Fitted Parameters and 95% Confidence Intervals

Parameters	This Work (Eq. 16)	Baird and Rama Rao (1991) (Eq. 7)
Mixing lengths (cm)		
l_b	3.20 ± 0.18	4.02
l_{do}	1.23 ± 0.32	—
l_m	0.34 ± 0.07	0.30
Weighting exponents		
n_b	0.495 ± 0.08	0.34
n_d	1.13 ± 0.34	—
Bass energy ϵ_{mo} (mW/kg)	6.85 ± 2.33	—

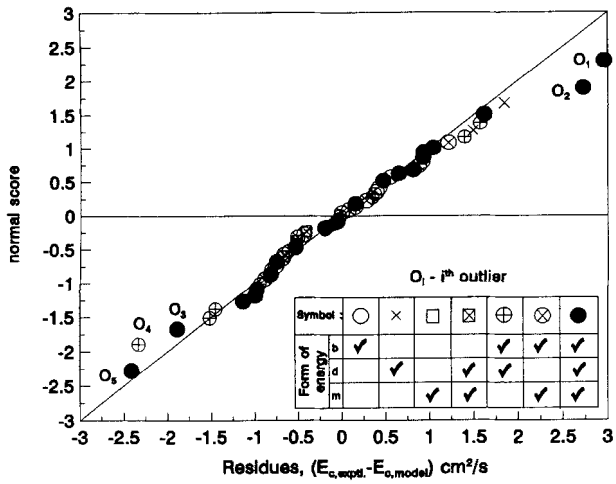

Figure 4. Normal probability plot of residuals.

cm^2/s^3). Further, the agitations were moderate and dispersed-phase flow was high. Under moderate agitation and high dispersed-phase flow, the circulation effects will be negligible and turbulent diffusion will not be high enough (under moderate total-energy dissipations) to cause such large values of E. Again, as explained later under moderately agitated conditions, the effects of buoyancy though still significant are lower relative to the case with no agitation. The reason for the high values is not quite clear. It is postulated that the increase could have been due a slight misalignment in the column verticality during this particular run.

2. Outliers 3–5 correspond to measurements of E at very low buoyant energy dissipations. These correspond to E measurements at the tail of the tracer concentration profile where ϵ_b values were less than 1 cm^2/s^3, which corresponded to an extremely small density difference of 0.0025 g/cm^3 in the continuous phase. Further, the concentrations were very low (less than 0.001 g/cm^3). In this region, slope estimations were subject to error. All these residuals were found to be negative, implying E_{pred} is greater than E_{expt}. The polynomial fit tended to flatten the curve at the tail region, so that the slopes were very close to zero, leading to higher values of E (Eq. 11). Manual slope estimations at the tail ends were even more error prone due to the very low concentrations and lack of sufficient number of points to localize the curve. The plots of residuals against the buoyant energy dissipation rate ϵ_b illustrated the preceding findings (Aravamudan, 1995).

The percentage error range associated with E is higher when compared to that of l. The estimation of E from the mixing length according to Eq. 3 includes the mixing-length term raised to the power of 4/3. Consequently, the error associated with l is magnified when Eq. 3 is used to find E. The magnification in percentage error with E with respect to l can be represented with reasonable accuracy according to Eq. 19.

$$M = \frac{\%\ \text{error}_E}{\%\ \text{error}_l} = \frac{86}{81} + \frac{26}{81}\frac{l_{\text{pred}}}{l_{\text{expt}}} - \frac{4}{81}\left(\frac{l_{\text{pred}}}{l_{\text{expt}}}\right)^2. \quad (19)$$

This result suggests that for a $\pm 20\%$ error in mixing length, the error in E is between $+25.8\%$ and -27.5%.

Implications of the Mixing-Length Model

Significance of the mixing-length terms

The model leads to three special cases where an individual mixing length becomes the only contributing factor to back-mixing, for example, when both ϵ_d and ϵ_m are zero, l equals l_b. Based on the parameter estimates, it can be seen that the effective mixing length l given by Eq. 16 can vary from a minimum value of l_m to a maximum of l_b even though the parameters l_m, l_b, and l_d (for a given dispersed phase flow and agitation rate) are constant. This is due to the weights attached to the different mixing-length terms. The weight refers to the ratio of a particular mode of energy dissipation rate (ϵ_b or ϵ_d) to the total energy dissipation rate ($\epsilon_b + \epsilon_d + \epsilon_m$). Hence the contribution to the back-mixing due to dispersed phase flow and buoyancy should not be viewed only in terms of the eddy scale associated with these two factors but also in terms of the fraction of their individual energy contribution to the overall energy dissipation. The exponents n_b and n_d on the fractional energy dissipation terms relate to the degree of the importance attached to the respective weights.

Table 4. Summary of Axial Mixing Models Using the Isotropic Turbulence Approach

Investigators	Baird and Rice (1975)	Holmes et al. (1991)	Baird and Rama Rao (1991)	This Work
Extraction apparatus	Bubble and spray columns	Karr-type RPC	Karr-type RPC	Karr-type RPC
Forms of energy dissipation	Dispersed phase	Buoyancy	Buoyancy + mechanical agitation	Buoyancy + dispersed phase + mechanical agitation
Eq. number	4	6	8	16
No. of mixing length parameters	1	1	2	3
No. of energy weighting exponents	0	0	1	2
Other parameters	0	0	0	1
Total adjustable parameters	1	1	3	6

The smaller the value of the exponent, the greater the influence of the weight and hence the mixing-length term. Hence as indicated by the estimated parameter n_b (Table 3), the buoyant energy dissipation effects caused by the unstable density gradients in the continuous phase are quite important despite their small magnitude. Further, the large value associated with l_b makes it very significant when buoyancy is the only factor contributing to back-mixing. The three weighted contributions can be expressed as follows, in units of cm:

$$L_m = l_m = 0.3363 \tag{20}$$

$$L_b = (l_b - l_m)\left(\frac{\epsilon_b}{\epsilon_b + \epsilon_m}\right)^{n_b} = 2.8628\left(\frac{\epsilon_b}{\epsilon_b + \epsilon_m}\right)^{0.4954} \tag{21}$$

$$L_d = \left[l_{do}\left(1 + \frac{H}{5.08}\right)\exp\left(-\frac{\epsilon_d}{\epsilon_{mo} + \epsilon_m}\right) - l_m\right]\left(\frac{\epsilon_d}{\epsilon_d + \epsilon_m}\right)^{n_d}$$
$$= \left[1.231\left(1 + \frac{H}{5.08}\right)\exp\left(-\frac{\epsilon_d}{68.52 + \epsilon_m}\right) - 0.3363\right] \times \left(\frac{\epsilon_d}{\epsilon_d + \epsilon_m}\right)^{1.13}, \tag{22}$$

so that the effective mixing length can now be expressed as

$$l = L_m + L_b + L_d. \tag{23}$$

Despite its apparent simplicity, this formulation contains important information. The eddies responsible for back-mixing are assumed to belong to the inertial subrange in which viscous effects are negligible and turbulence is only determined by the specific energy dissipation rate. A spectrum of eddy scales is possible in this region due to the exchange of momentum between the eddies generated by different sources of energy dissipation. The scale L_m represents the smallest eddies present in the inertial subrange created by the interaction of eddies from different sources of energy dissipation. This class is mainly due to mechanical agitation. The remaining two classes of eddies generated by dispersed-phase and buoyant-energy dissipations are represented by L_d and L_b, weighted according to their respective fractional energy contributions. However, when there is only one source of energy dissipation, it is assumed that the eddies in the inertial subrange are similar in scale and can be represented by l_b, l_d, or l_m, depending on the source of energy dissipation. Experimental data were used to determine the scales of these eddies.

The scale L_m (= 0.3363 cm) is comparable to the value of 0.30 cm reported by Baird and Rama Rao (1991) for single-phase flow conditions. It can be seen from Table 3 that the mixing lengths l_b and l_m are of the same order of magnitude as in the earlier work of Baird and Rama Rao (1991), which was entirely under single-phase conditions.

The buoyant-energy mixing length (l_b) constitutes 63% of the column diameter and is in the same order of values obtained by earlier workers. The value of l_b corresponding to Holmes et al. (1991) work in a 7.6-cm-diameter Karr column is 70% of the column diameter, while Baird and Rama Rao (1991) reported values close to 80%. The weighting exponent n_b was 0.34 in their work, while it is close to 0.5 in the present work. The data of Holmes et al. (1991) and Baird and Rama Rao (1991) focused only on the single-phase situation, while the present work had only a limited amount of single-phase data and focused mainly on two phase flow conditions.

The dispersed-phase mixing length (l_d), unlike the previous terms, is variable and dependent on dispersed- and mechanical-energy dissipations and plate spacing. In previous studies on bubble columns, the mixing-length concept has often been used to describe back-mixing in the continuous phase. Kawase and Moo-Young (1986) assumed that the mixing length for two-phase flow was substantially similar to that for a single-phase flow and obtained the average mixing length equal to 10% of the column diameter. Kawase and Tokunaga (1991) used data on bubble columns covering a wide range of column diameters ($0 < D \leq 0.6$ m) and superficial gas velocities ($0.01 \leq u_{sg} \leq 1.45$ m/s). The average mixing length was obtained by integrating the equation governing the radial variation of the velocity in the turbulent core and regressing the available experimental data. The following correlation for the average mixing length was proposed

$$l_{\text{mean}} = 4.5 \times 10^{-2} u_{sg}^{-0.38} D. \tag{24}$$

This is qualitatively similar to the results in the present work, which accounts for the decrease in mixing length with dispersed-phase flow velocity. The characteristic mixing length l_d is less than the value 2.2 cm that would be expected from Eq. 5 for an open column (Baird and Rice, 1975). However, it should be noted that the current model Eq. 13 contains an exponential term and a term in H/D, so direct comparison is not possible.

In the present work, the model can also be qualitatively interpreted in terms of the ideas proposed by Rice and coworkers (1987, 1992). Rice and Littlefield (1987) in their back-mixing studies in a 14-cm-diameter bubble column observed that even a slight tilt in the alignment of the column produced excessive back-mixing. In a perfectly vertical column under ideal bubbly flow conditions the mixing-length scale in the isotropic turbulence model was proportional to the bubble size, which was uniform at 0.41 cm. Rice and Littlefield observed that this scale can become larger, tending toward the column diameter as the conditions changed from homogeneous bubbly regime to heterogeneous churn-turbulence regime. In the present work, the drop-size distribution under nonagitated conditions was nonuniform and closer to the churn-turbulent regime. Hence, the dispersed-phase mixing lengths were always larger than the drop diameters.

Geary and Rice (1992) discussed the possibility of mixing in the continuous phase due to (1) turbulence generated near the wall propagating to the core of the liquid, in addition to (2) the turbulence created by the bubble motion. The authors recommended choosing the mixing scale that leads to minimizing the dissipation in the continuous phase, that is, when the larger of the two mixing scales is chosen. The model developed in this work can also be interpreted to take into account both terms of the turbulence generated at the wall (and its corresponding mixing length) and the turbulence generated due to drops. At zero agitation and low dispersed-phase flow rates, circulation of the continuous phase in the proximity of the wall generates turbulence that propagates to the

the core of the column. This contributes mainly to the effective dispersed-phase mixing length l_d. At higher dispersed-phase flows this latent turbulence is damped out by the dense dispersion of drops present in the core and the effect of the wall is weakened. At very high dispersed-phase flows eddy dispersion generated by the drops dominates the disperse phase back-mixing contribution. The same comments apply when the effects of mechanical agitation are considered; as it is increased, the relative effect of the wall turbulence is reduced.

Hence, three regimes can be proposed to explain the dispersed-phase contribution to the back-mixing in the continuous phase. For the sake of convenience in illustration it is assumed that the buoyant energy dissipation effects are absent, that is, $\epsilon_b = 0$.

1. Circulation Regime I (zero mechanical agitation and low dispersed phase flow rate)

$$E = \left(l_{do}^{*} \left(1 + \frac{H}{D} \right) \exp\left(- \frac{\epsilon_d}{\epsilon_{mo}} \right) \right)^{4/3} \epsilon_d^{1/3}. \qquad (25)$$

In this regime, the total dispersed-phase energy dissipation is quite low and turbulent eddy diffusion is less important than the circulation effects. In this regime, l_d is maximum and $\epsilon_t^{1/3}$ is low.

2. Intermediate Regime II (zero mechanical agitation and high dispersed-phase flow). In this regime, the exponential term decays rapidly and l_d decreases as well. The circulation effects are quickly damped out and the eddy dispersion term becomes important due to the increase in ϵ_d and hence in $\epsilon_t^{1/3}$. This corresponds to a region when the back-mixing coefficient passes through a minimum with respect to dispersed-phase flow.

3. Eddy Diffusion Regime III (nonzero agitation). In this regime, the dispersed-phase flow rate is no longer the critical factor. The exponential term in Eq. 16 tends asymptotically toward unity with increasing agitation thereby marking a shift in the operating regime of the column. The circulation effects are absent and the total energy-dissipation term $(\epsilon_m + \epsilon_d)^{1/3}$ increases rapidly, leading to eddy dispersion in the core of the column becoming very important. The back-mixing coefficients are higher than those in the intermediate regime if not higher than those corresponding to the regime *I*. For a given column geometry, l_d tends toward a constant value.

The model parameters (especially ϵ_{mo} and l_d) are only valid in the range of dispersed-flow rates investigated. Extending this model beyond the limits in this work may lead to erroneous results.

Contribution of Wakes to Back-Mixing

The model just described contains the contributions of unstable density gradient and mechanical agitation (leading to eddy turbulent dispersion) and dispersed-phase flow (leading to circulatory flow at low values and eddy dispersion at high flows). However, the influence of wakes has not been incorporated in detail. The importance of wakes in the overall back-mixing process seems to be less than that of circulatory flow (Anderson and Pratt, 1978; Steiner and Hartland, 1983). To include the contribution of wakes into the back-mixing model in detail would require additional parameters like wake volume, wake shedding height, and droplet volume (Steiner and Hartland, 1983). These parameters are difficult to estimate, particularly under agitated conditions. Further, in cocurrent flow both the dispersed and continuous phase are flowing in the same direction. Hence the wakes will consist of the continuous phase being transported in the same direction as the bulk flow of the continuous phase. Hence there is no contribution of wake transport to back-mixing in cocurrent flow situations.

Effect of the Buoyant-Energy Dissipation Rate

Overal statistical comparisons such as those shown in Figure 4 do not provide direct information on the effects of individual variables. In this section these effects are examined, both in terms of predicted trends from Eq. 16 and actual data points.

Single-phase flow conditions

The effect of ϵ_b is illustrated in Figure 5 using ϵ_m as the parameter (which includes the effect of plate spacing according to Eq. 8). Three levels of energy dissipation are plotted: zero, moderate ($0 < \epsilon_m < 3{,}500$ cm^2/s^3), and high ($3{,}500 < \epsilon_m < 17{,}500$ cm^2/s^3). Typical ranges of ϵ_m had to be considered and the individual data points are labeled in the figure with the applicable values of ϵ_m. From the trends shown in the figure, it can be seen that even when the buoyant-energy dissipations are very small (0–10 cm^2/s^3) when compared to the rates of the mechanical-energy dissipation (0–8,000 cm^2/s^3), they produce a significant enhancement in E. Even a very small unstable density gradient in the continuous phase can significantly increase axial mixing. The effect of buoyancy is predominant at zero mechanical agitation.

With increasing agitation, the effective mixing length decreases and is in the range $l_m < l < l_b$. Under moderate agitation, E decreases relative to the case when $\epsilon_m = 0$. At increasing mechanical agitation, l tends toward the limiting

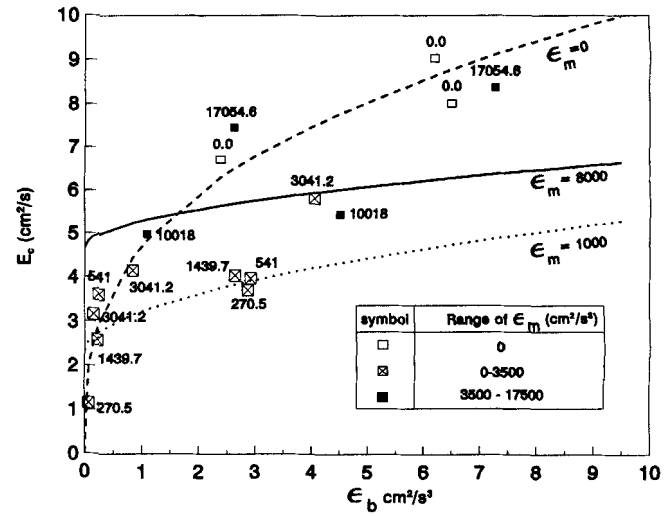

Figure 5. Variation of back-mixing coefficient with buoyant energy dissipation (single-phase flow conditions).

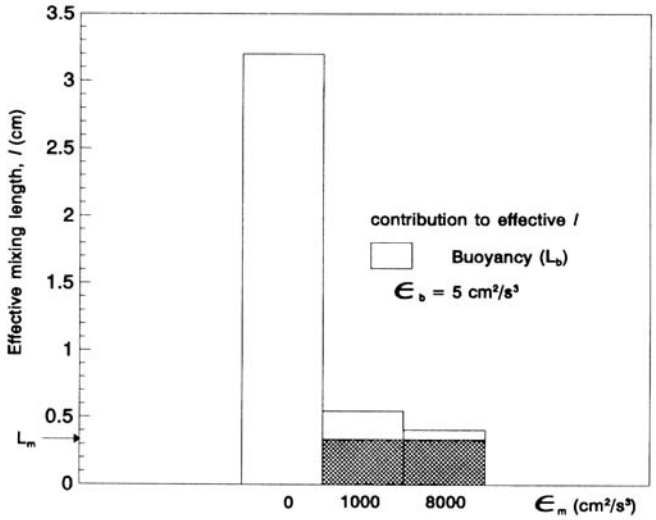

Figure 6. Relative contributions of buoyancy and mechanical agitation to effective mixing length under single-phase flow conditions.

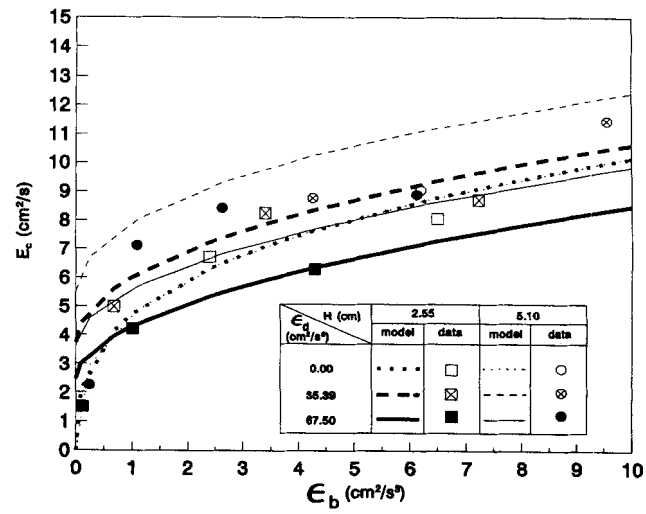

Figure 7. Variation of back-mixing coefficient with buoyant energy dissipation (two-phase flow unagitated conditions).

constant value l_m, and since total energy dissipation ϵ_t ($= \epsilon_m + \epsilon_b$) is high, E defined by Eq. 3 starts to increase again. Hence as shown in Figure 5, E passes through a minimum with respect to ϵ_m before starting to increase. The effect of increasing mechanical energy dissipation on the effective mixing length l for an average value of $\epsilon_b = 5$ cm^2/s^3 is illustrated in Figure 6. As can be observed from this figure, the model predicts that with the presence of mechanical energy dissipation, the effective contribution of the buoyancy term to the effective mixing length is reduced. At intense mechanical agitation, the small eddies of high intensity predominate over the larger eddies of much smaller energy intensity generated by the buoyancy effects, and the mixing length tends toward l_m.

Two-phase flow conditions

Under these conditions, there is an additional contributing factor to turbulence, viz., the dispersed-phase energy dissipation (ϵ_d). First, the situation corresponding to no mechanical agitation (ϵ_m) is discussed. The parameters are ϵ_d and plate spacing H. Two levels of ϵ_d and H are used. Since the variation of the experimental ϵ_d from either of the two levels was very small, the data points are not labeled in Figure 7. The situation corresponding to zero dispersed-phase flow is also shown for comparison. The results illustrated in Figure 7 show that the buoyant energy dissipation is still important under two-phase flow conditions. The trend of increase in E with ϵ_b is similar irrespective of the dispersed-phase energy dissipation and plate spacing. In addition to these effects, it can also be noted that the E values are strongly influenced by the dispersed-phase energy dissipation and plate spacing as discussed earlier.

The relative significance of buoyancy and dispersed-phase contributions at different plate spacings is illustrated in Figure 8. The value of ϵ_b is fixed at a typical 5 cm^2/s^3. The effective mixing length decreases with increasing dispersed-phase flow at a given plate spacing due to the attenuation in the circulation effects, as explained previously. Further, the weight $\epsilon_b/(\epsilon_b + \epsilon_d)$ is reduced with increasing ϵ_d, thereby diluting the contribution of the buoyancy effect. It is interesting to note that L_b and L_d are comparable despite the order of magnitude difference between the two forms of energy dissipations. The model estimates of n_b ($= 0.4954$) and n_d ($= 1.13$) attribute a heavier weight to the buoyancy term. Further, the value of the exponent n_d tends to reduce the weight attached to the dispersed-phase mixing length and hence its contribution to the overall mixing length, in spite of the high fraction of ϵ_d/ϵ_t. These factors, considered along with a high value of l_b, result in a significant enhancement in the back-mixing coefficient due to the buoyancy. Based on the observations made in this and previous studies, if the concept of buoyancy mixing length being 60–80% of column diameter

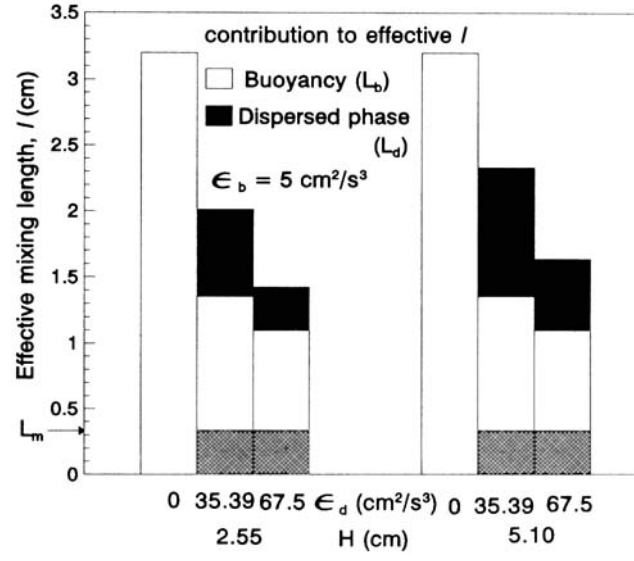

Figure 8. Relative contributions of buoyancy and dispersed-phase flow to effective mixing length under two-phase flow unagitated conditions.

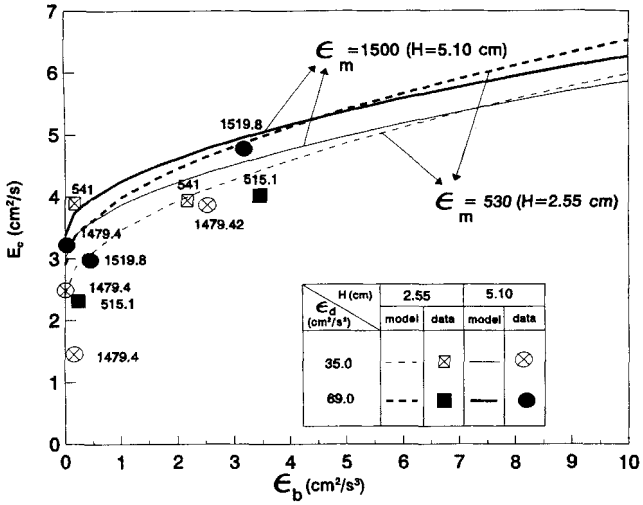

Figure 9. Variation of back-mixing coefficient with buoyant energy dissipation (two-phase flow moderately agitated conditions).

can be extended to commercial spray columns of much larger diameter, the back-mixing effects in such columns due to buoyancy would be expected to be severe.

Effect of buoyancy under two-phase-flow agitated conditions (ϵ_b, ϵ_m and $\epsilon_d > 0$)

These conditions approximate closely to the actual industrial situation except that mass transfer is not present. Typical model trends are shown in Figures 9 and 10. Low and moderate mechanical-energy dissipations of 530 and 1,500 cm^2/s^3 corresponding to plate spacings 2.55 and 5.10 cm, respectively, are shown in Figure 9, and intense mechanical-energy dissipation of 15,000 cm^2/s^3 corresponding to a plate spacing of 2.55 cm is shown in Figure 10. Single-phase flow E values are also shown in the latter figure for comparison. Since the experimental ϵ_m varied around the values used in

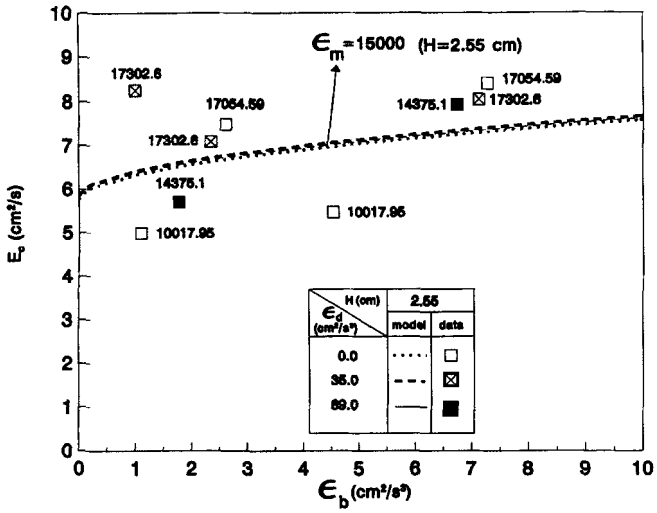

Figure 10. Variation of back-mixing coefficient with buoyant energy dissipation (two-phase flow intensely agitated conditions).

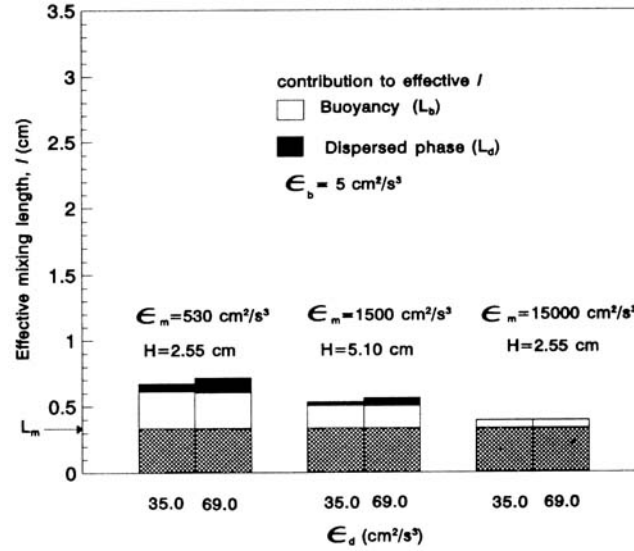

Figure 11. Relative contributions of buoyancy, dispersed-phase flow, and mechanical agitation to effective mixing length under two-phase flow agitated conditions.

the model trends, they were labeled in the figures. The conclusions drawn based on these results are discussed below.

At low and moderate agitations ϵ_b still has an important effect in enhancing E. It can be seen that under conditions of intense mechanical agitation, the enhancement in E due to buoyancy effects is still evident even though it is attenuated and E tends toward a constant value as in single-phase flow.

It can be observed that the influence of ϵ_d on E is stronger at lower levels of mechanical agitation. As ϵ_m increases, the difference between E values at different dispersed-phase flows narrows down as shown in Figure 9. As explained before, the dispersed-phase mixing length l_d tends toward a constant value since the exponential term approaches unity. At intense mechanical agitation, E attains a constant value, insensitive to ϵ_d (Figure 10) and approaching single-phase values. This is consistent with previous work in the absence of density gradients, for example, Kim and Baird (1976). When comparing the contributions of the buoyancy- and dispersed-phase flow it can be seen from Figure 11 that at low agitations the dispersed-phase contribution to the effective mixing length is lower than that of the buoyancy effects.

It is interesting to note from Figure 9 that a column operating with a plate spacing of 5.10 cm accompanied by a mechanical-energy dissipation of 1,500 cm^2/s^3 ($f = 1.87$ Hz) experiences nearly equivalent back-mixing to that of a column operating with a plate spacing of 2.55 cm and mechanical-energy dissipation of 530 cm^2/s^3 ($f = 1.0$ Hz). This suggests that the use of a higher plate spacing enables the column to operate at higher agitation levels without a serious deterioration in the back-mixing effects.

Conclusions

Effects of unstable density gradient

The effect of unstable density gradients on axial dispersion under two-phase flow conditions has been investigated sys-

tematically for the first time. This study confirms earlier concerns (Cusack and Karr, 1991) about increased mixing when the continuous phase density increases with vertical height in a column. Unstable density gradients can significantly increase axial mixing and have the greatest effects at low mechanical-agitation rates or in the absence of mechanical agitation (Figures 5 and 7). Even under well-agitated conditions the value of E can be increased up to 25% in the presence of an unstable density gradient (Figure 10).

Modeling

The Kolmogoroff isotropic turbulence model has been adopted to take account of the effects of three different variables on axial mixing: mechanical agitation, the flow of the dispersed phase, and unstable density gradients. The new model, given by Eq. 16, contains six adjustable parameters. One parameter (a mixing length l_m) is associated with the mechanical-energy input and corresponds to the eddies formed by reciprocating the column plates. It is also representative of the smaller eddy scales formed by the turbulent energy spectrum created by buoyancy and dispersed-phase energy dissipations. The effects of dispersed-phase flow are described in the model by a mixing length l_d, an energy level that determines the effect of mechanical agitation (ϵ_{mo}) in reducing circulation effects and a weighting exponent n_d. The effects of unstable density gradient are accounted for by a mixing length l_b and a weighting exponent n_b. Values of the six parameters have been determined statistically from the data and are given in Table 3. Table 4 summarizes axial mixing models using the isotrophic turbulence approach.

The mixing model is based on specific energy-dissipation rates and assumed mixing lengths. Although energy-dissipation rates due to unstable density gradients are relatively low, the model accounts for their large effect by assigning a larger value to the effective mixing length for this type of energy dissipation. The effect of the dispersed-phase flow on axial mixing is partly associated with circulation due to transverse nonuniformity; this is particularly so at low dispersed-phase flow rates and low mechanical-energy inputs. The circulation effects have been incorporated into the mixing-length model as discussed in detail earlier in the article.

Practical implications

Literature correlations, and most experimental data for axial dispersion, refer to conditions in which the continuous-phase density is independent of height. This work has shown that if the density increases with height, mixing will be enhanced. This could in turn lead to a poorer than expected separation performance under countercurrent conditions. The mixing length for buoyant mixing (like that for the dispersed-phase flow) is believed to increase with column diameter, and that suggests that the effect of unstable-density gradient will be greater at larger scales. It is recommended that in the design of large-scale columns, process conditions should if possible be set so that unstable density gradients do not occur.

Another practical implication concerns laboratory measurements of continuous-phase axial mixing using tracers, either under steady or unsteady conditions. Precautions are usually taken to ensure that the tracer solution density is close to that of the continuous phase, but this work has shown that even a small unstable density difference, in the order 0.001 g/mL, can increase axial dispersion.

Recommendations

This work has been carried out under cocurrent conditions, and it is recommended that further work should be carried out under countercurrent conditions, preferably in the presence of mass transfer. It is also recommended that the effects of a stable density gradient (i.e., continuous-phase density decreasing with vertical distance) on mixing should be studied. It is possible that a stable density gradient could reduce axial dispersion and therefore have a beneficial effect on separation efficiency, but the extent of this effect is not yet known.

Acknowledgment

This work was supported by a Research Grant from the Natural Sciences and Engineering Research Council of Canada.

Notation

c = tracer concentration, kg/m^3
C_o = orifice coefficient
D = diameter of the column, m
E = axial or back-mixing coefficient in the continuous phase, m^2/s
E_a = axial or back-mixing coefficient due to agitation, m^2/s
E_{tn} = axial or back-mixing coefficient due to transverse nonuniformity, m^2/s
f = frequency of oscillation, Hz
g = gravitational acceleration of value 9.80665, m/s^2
H = plate spacing or stage height, m
l_b = buoyancy mixing length, m
l_d = dispersed phase mixing length, m
l_{do} = dispersed phase mixing length defined in Eq. 14, m
l^*_{do} = resolved dispersed-phase mixing length given in Eq. 14, m
L_b = weighted contribution of the buoyancy effect defined by Eq. 21, m
L_d = weighted contribution of the dispersed effect defined by Eq. 22,. m
L_f = flooding ratio given by u_d/u_c
L_m = limiting mixing length as defined by Eq. 20, m
M = magnification factor, defined in Eq. 19
N = mass or molar flux in the axial direction, kg/m^2·s or kmol/m^2·s
n_b = exponent in the fractional power dissipation rate term for buoyancy
n_d = exponent in the fractional power dissipation term for dispersed phase flow
O_i = outlier
s = standard deviation
u = superficial velocity, m/s

Greek letters

β^* = length of the circulation cell referred in Eq. 13, m
Δ = difference operator between two quantities
ϵ = energy dissipation rate, m^2/s^3
ϵ_b, ϵ_d = buoyant-specific and dispersed-phase specific energy-dissipation rate, m^2/s^3
ϵ_m, ϵ_t = mechanical-agitation-specific and total-agitation-specific energy-dissipation rate, m^2/s^3
ρ = density, kg/m^3
ρ_c = density of the continuous phase, kg/m^3
ρ_{co} = density of continuous phase with zero tracer concentration, kg/m^3
$\Delta\rho$ = density difference in the continuous phase, kg/m^3

Subscripts

b = buoyancy
c = continuous
d = dispersed
expt = experimental
m = mechanical
o = orifice or hole of plate
pred = predicted

Literature Cited

Anderson, W. J., and H. R. C. Pratt, "Wake Formation and Circulatory Flow in Bubble and Droplet-Type Contactors," *Chem. Eng. Sci.*, **33**, 995 (1978).

Aravamudan, K., "Back-mixing Studies in the Presence of an Unstable Density Gradient in a Reciprocating Plate Extraction Column," PhD Thesis, McMaster Univ., Hamilton, Ontario, Canada (1995).

Baird, M. H. I., K. Aravamudan, N. V. Rama Rao, J. Chadam, and A. P. Pierce, "Unsteady Axial Mixing by Natural Convection in a Vertical Column," *AIChE J.*, **38**, 1825 (1992).

Baird, M. H. I., and B. A. Legree, "Natural Convection Heat Transfer from Open Vertical Tubes," *Can. J. Chem. Eng.*, **72**, 755 (1994).

Baird, M. H. I., and N. V. Rama Rao, "Axial Mixing in a Reciprocating Plate Column in Presence of Very Small Unstable Density Gradient," *AIChE J.*, **37**, 1019 (1991).

Baird, M. H. I., N. V. Rama Rao, J. Prochazka, and H. Sovova, "Reciprocating-Plate Columns," *Liquid-Liquid Extraction Equipment*, J. C. Godfrey and M. J. Slater, eds., Wiley, New York, p. 307 (1994).

Baird, M. H. I., and R. G. Rice, "Axial Dispersion in Large Unbaffled Columns," *Chem. Eng. J.*, **9**, 171 (1975).

Bensalem, A. K., "Hydraulics and Mass Transfer in a Reciprocating Plate Column," PhD Thesis, Swiss Federal Inst. Tech., Zürich (1985).

Cusack, R. W., and A. Karr, "A Fresh Look at Liquid-Liquid Extraction," *Chem. Eng.*, **4**, 112 (1991).

Devanathan, N., D. Moslemian, and M. P. Dudukovic, "Flow Mapping in Bubble Columns Using CARPT," *Chem. Eng. Sci.*, **45**, 2285 (1990).

Dongaonkar, K. R., H. R. C. Pratt, and G. W. Stevens, "Mass Transfer and Axial Dispersion in a Kühni Extraction Column," *AIChE J.*, **37**, 694 (1991).

Draper, N. R., and H. Smith, "The Examination of Residuals," *Applied Regression Analysis*, 2nd ed., Wiley, New York, p. 141 (1981).

Geary, N. W., and R. G. Rice, "Circulation and Scale-Up in Bubble Columns," *AIChE J.*, **38**, 76 (1992).

Hafez, M. M., M. H. I. Baird, and I. Nirdosh, "Flooding and Axial Dispersion in Reciprocating Plate Extraction Columns," *Can. J. Chem. Eng.*, **57**, 150 (1979).

Hafez, M. M., and M. H. I. Baird, "Power Consumption in a Reciprocating Plate Extraction Column," *Trans. Inst. Chem. Eng.*, **56**, 229 (1978).

Holmes, T. L., A. E. Karr, and M. H. I. Baird, "Effect of Unfavourable Density Gradient on Axial Mixing," *AIChE J.*, **37**, 360 (1991).

Joshi, J. B., and M. M. Sharma, "A Circulation Model for Bubble Columns," *Trans. Inst. Chem. Eng.*, **57**, 244 (1979).

Karr, A. E., "Performance of a Reciprocating-Plate Extraction Column," *AIChE J.*, **5**, 446 (1959).

Karr, A. E., S. Ramanujam, T. C. Lo, and M. H. I. Baird, "Axial Mixing and Scale-up of Reciprocating Plate Extraction Column," *Can. J. Chem. Eng.*, **65**, 373 (1987).

Kawase, Y., and M. Moo-Young, "Liquid Phase Mixing in Bubble Columns with Newtonian and Non-Newtonian Fluids," *Chem. Eng. Sci.*, **41**, 1969 (1986).

Kawase, Y., and M. Tokunaga, "Characteristic Mixing Length in Bubble Columns," *Can. J. Chem. Eng.*, **69**, 1228 (1991).

Kawase, Y., and M. Moo-Young, "Mathematical Models for Design of Bio-reactors: Applications of Kolmogoroff's Theory of Isotropic Turbulence," *Chem. Eng. J.*, **43**, B19 (1990).

Kim, S. D., and M. H. I. Baird, "Axial Dispersion in a Reciprocating Plate Extraction Column," *Can. J. Chem. Eng.*, **54**, 81 (1976).

Kolmogoroff, A. N., "The Local Structure of Turbulence in Incompressible Viscous Fluid for Very Large Reynolds Numbers," *Akad. Nauk U.S.S.R.*, **30**, 301 (1941).

Kostanyan, A. E., V. L. Pebalk, and T. K. Pelevina, "Energy Consumption and Dispersion in Extractors with Vibrating Plates," *Teor. Osn. Khim. Tekhnol.*, **13**, 624 (1979).

Lo, T. C., and J. Prochazka, "Reciprocating Plate Extraction Columns," *Handbook of Solvent Extraction*, T. C. Lo, M. H. I. Baird, and C. Hanson, eds., Wiley-Interscience, New York, p. 373 (1983).

Nemecek, M., and J. Prochazka, "Longitudinal Mixing in a Vibrating Column: Two Phase Flow," *Can. J. Chem. Eng.*, **52**, 739 (1974).

Novotny, P., J. Prochazka, and J. Landau, "Longitudinal Mixing in Reciprocating and Pulsed Sieve Plate Column: Single Phase Flow," *Can. J. Chem. Eng.*, **48**, 405 (1970).

Pratt, H. R. C., and M. H. I. Baird, "Axial Dispersion," *Handbook of Solvent Extraction*, T. C. Lo, M. H. I. Baird, and C. Hanson, eds., Wiley-Interscience, New York, p. 199 (1983).

Rice, R. G., and M. A. Littlefield, "Dispersion Coefficients for Ideal Bubbly Flow in Truly Vertical Bubble Columns," *Chem. Eng. Sci.*, **42**, 2045 (1987).

Rod, V., "Calculating Mass Transfer with Longitudinal Mixing," *Brit. Chem. Eng.*, **11**, 483 (1966).

Rosen, A. M., and V. S. Krylov, "The Scaling Up of Mass Transfer Equipment and Reactors: Use of Hydraulic Model Experiments," *Chem. Eng. Sci.*, **22**, 407 (1967).

Rosen, A. M., and V. S. Krylov, "Theory of Scaling Up and Hydrodynamic Modelling of Industrial Mass Transfer Equipment," *Chem. Eng. Sci.*, **7**, 85 (1974).

Sege, G., and F. W. Woodfield, "Pulse-Column Variables," *AIChE Symp. Ser.*, **50**, 179 (1954).

Steiner, L., and S. Hartland, "Hydrodynamics of Liquid-Liquid Spray Columns," *Handbook of Fluids in Motion*, N. P. Cheremisinoff and R. Gupta, eds., Ann Arbor Science, Ann Arbor, MI, p. 1049 (1983).

Stevens, G. W., and M. H. I. Baird, "A Model for Axial Mixing in Reciprocating Plate Columns," *Chem. Eng. Sci.*, **45**, 457 (1990).

Treybal, R. E., *Liquid Extraction*, 2nd ed., McGraw-Hill, New York (1963).

Walter, J. F., and H. W. Blanch, "Liquid Circulation Patterns and their Effect on Gas Holdup and Axial Mixing in Bubble Columns," *Chem. Eng. Commun.*, **19**, 243 (1983).

Manuscript received Apr. 5, 1995, and revision received Nov. 27, 1995.